J Inorg Organomet Polym (2013) 23:147–157
DOI 10.1007/s10904-012-9727-3

Ferrocene-Decorated Hyperbranched Poly(aroxycarbonylphenylene)s: Synthesis, Light Refraction, Photopatterning and Precursor to Magnetic Ceramics

Cathy K. W. Jim · Jacky W. Y. Lam · Anjun Qin · Chris W. T. Leung · Liu Jianzhao · Herman H. Y. Sung · Ian D. Williams · Ben Zhong Tang

Received: 29 June 2012 / Accepted: 27 July 2012 / Published online: 14 August 2012

Abstract Ferrocene-decorated hyperbranched poly[1,3,5-tri(aroycarbonyl)phenylene]s (*hb*-PTACPs) are prepared in moderate yields with high molecular weights by one-pot polycyclotrimerization of 4,4′-isopropylidenediphenyl bipropiolate with 4-(ferrocenylmethyl)phenyl propiolate in reflux dimethylformamide. All the polymers are soluble and film-forming. They enjoy high thermal stability and lost little of their weight when heated to 300 °C under nitrogen. Thin solid films of the organometallic polymers shows high refractive indices (RI = 1.7038–1.6295) in the wavelength region of 400–1,700 nm. Ceramization of the organometallic *hb*-PTACPs at high temperature under inert atmosphere gives iron nanoparticles with high magnetizabilities. The organometallic polymers are readily crosslinked under UV irradiation and pyrolysis of the patterned polymer films produces magnetic ceramic patterns with good shape retention.

This article is dedicated to Dr. Hiroshi Nishihara on his outstanding contribution to the field of metal-containing polymer.

Electronic supplementary material The online version of this article (doi:10.1007/s10904-012-9727-3) contains supplementary material, which is available to authorized users.

C. K. W. Jim · J. W. Y. Lam · C. W. T. Leung · L. Jianzhao · H. H. Y. Sung · I. D. Williams · B. Z. Tang (✉)
Department of Chemistry, Fok Ying Tung Research Institute, Institute for Advanced Study, State Key Laboratory of Molecular Neuroscience, Institute of Molecular Functional Materials and Division of Biomedical Engineering, The Hong Kong University of Science & Technology, Clear Water Bay, Kowloon, Hong Kong, China
e-mail: tangbenz@ust.hk

A. Qin
Department of Polymer Science & Engineering, Zhejiang University, Hangzhou 310027, China

Keywords Ceramics · Ferrocene · Hyperbranched polymer · Magnetism · Photopattern · Refractive index

1 Introduction

Macroscopically processable polymers with high refractive indices (RI's) are promising candidate materials for applications in photonic and optoelectronic devices [1, 2]. Organometallic polymers are hybrid macromolecules of organic and inorganic species and exhibit unique magnetic, electronic, catalytic, sensoric, and optical properties [3–15]. They also show high RI values but they, on the other hand, generally possess low processability, which makes them not well suited to the manufacture of large area flat-panel devices. Organic polymers show good solubility in solvents and film-forming capability. The RI values for most of conventional organic polymers, however, lie in between ~1.40 and ~1.65, with the majority located in a very narrow range of ~1.5–1.6. For example, poly(methyl methacrylate), polycarbonate and polystyrene are the well-known optical glasses [16] but exhibit RI values of merely 1.491, 1.581 and 1.590, respectively at 589.3 nm. Very few polymers show RI values higher than 1.70. The low refractivities of the existing organic polymers have significantly limited their practical applications and largely retarded the progress in the development of organic photonic systems.

Theory predicts that macromolecules containing groups or units with high polarizabilities and small molecular volumes may show high light refractivities. Indeed, we found that functional polymers constructed from acetylenic building blocks exhibited much higher RI values than those of conventional polymers mentioned above [17–23]. For example, hyperbranched poly[1,3,5-tri(aroycarbonyl)phenylene]s (*hb*-PTACPs) prepared by polycyclotrimerization of

bipropiolates in reflux dimethylformamide (DMF) showed high RI values (1.6255–1.681) in a wide wavelength region of 400–1,700 nm with very low optical dispersion ($D' = 0.00097$) [22]. Coupled with their high optical transparency, they are anticipated to find high-tech applications as coating materials in the advanced display systems such as microlens components for charge-coupled devices and high performance CMOS image sensors [24–27].

Photonic materials containing metallic species, Group VI elements (Si, Ge, Sn and Pb) and heavy atoms (Br, I, P and S) generally show high RI values. In this work, to enhance further the RI of *hb*-PTACPs as well as endow them with new and/or enhanced properties, we explore the possibility of incorporation of transition metals into the polymer structures. We choose ferrocene (Fc) as the integrated species because of its high stability and the well-established methods for its incorporation into more complex structures as well as novel materials properties [28–37]. We herein show that the copolymerization of bipropiolate (**1**) and organometallic monopropiolate (**16**) can be effectively initiated in reflux DMF without adding any external catalysts, producing processable organometallic *hb*-PTACPs with high molecular weights in moderate yields (Scheme 1). Instead of exhibiting high RI and good photopatternability inherent from the parent polymer, the organometallic *hb*-PTACPs P**1/2** can be pyrolyzed to give ferromagnetic materials and magnetoceramic pattern, thanks to the Fc units in the polymers.

2 Experimental

2.1 Materials

4,4′-Isopropylidenediphenyl bipropiolate (**1**) was prepared according to the published experimental procedures [22]. Tetrahydrofuran (THF; Labscan) was distilled under

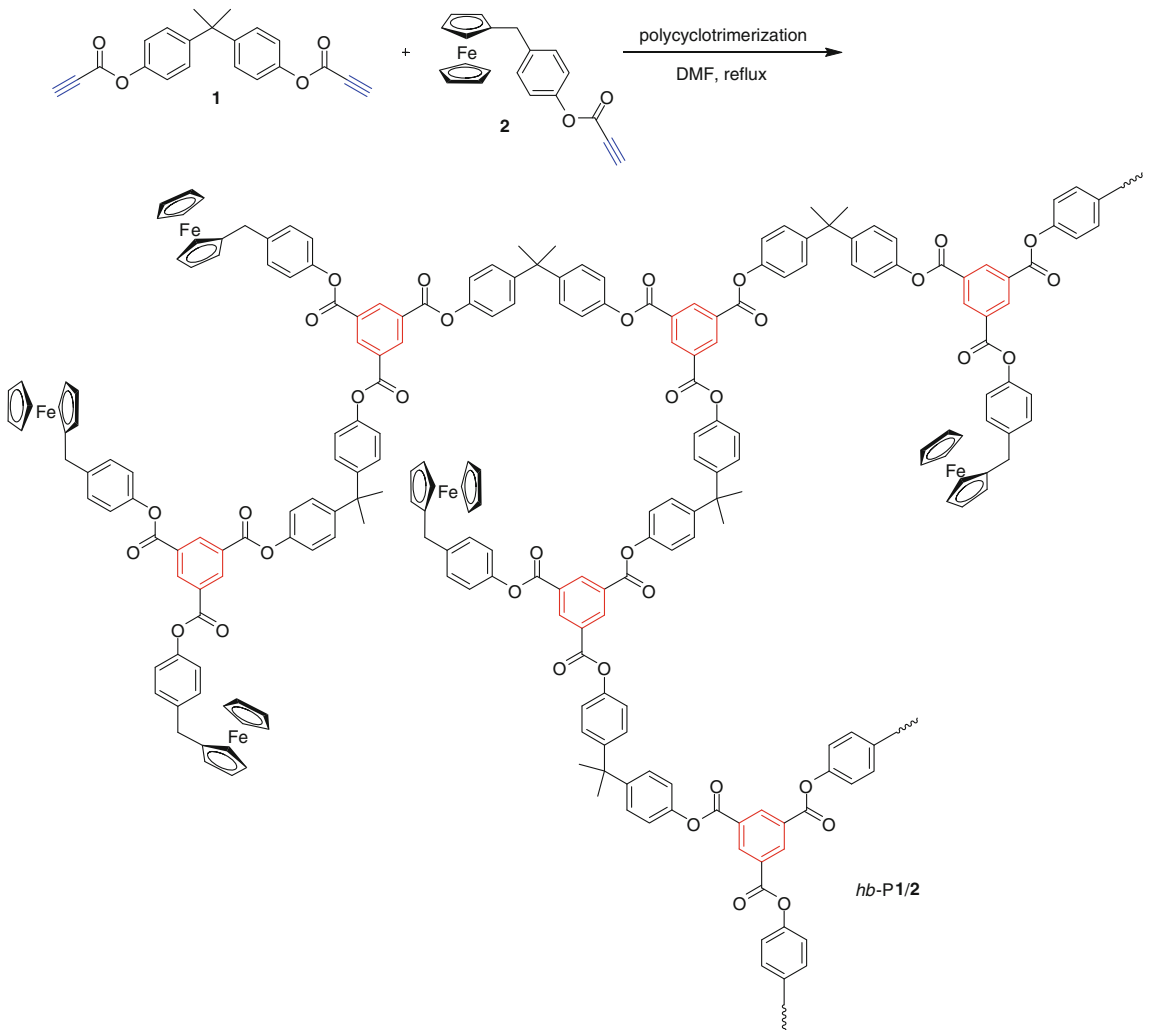

Scheme 1 Construction of organometallic hyperbranched polymers by copolycyclotrimerization of bipropiolate **1** with monopropiolate **2**

nitrogen from sodium benzophenone ketyl immediately prior to use. All other solvents were purified using standard procedures. Ferrocene (**3**), 4-methoxybenzyl alcohol (**4**), propiolic acid (**7**), 1,3-dicyclohexylcarbodiimide (DCC), 4-(dimethylamino)pyridine (DMAP), *p*-toluenesulfonic acid monohydrate (TsOH) and other chemicals were purchased from Aldrich and used as received without further purification.

2.2 Instrumentation

Number- (M_n) and weight- (M_w) averaged molecular weights and polydispersity indices (M_w/M_n) of the polymers were estimated by a Waters Associates Gel Permeation Chromatography (GPC) system equipped with RI and UV detectors. THF was used as eluent at a flow rate of 1.0 mL. A set of linear polystyrenes was used for the molecular weight calibration. IR spectra were recorded on a Perkin-Elmer 16 PC FT-IR spectrophotometer. ^{1}H and ^{13}C NMR spectra were measured on a Bruker ARX 300 NMR spectrometer using $CDCl_3$ or dimethylsulfoxide (DMSO)-d_6 as solvent. Single crystal X-ray diffraction intensity data were collected at 100 K on a Bruker-Nonices Smart Apex CCD diffractometer with graphite monochromated Mo Kα radiation. Processing of the intensity data was carried out using the SAINT and SADABS routines, and the structure and refinement were conducted using the SHELTL suite of X-ray programs (version 6.10). UV spectra were measured on a Milton Roy Spectronic 3000 array spectrophotometer. Thermogravimetric analyses (TGA) were carried out under nitrogen on a Perkin-Elmer TGA 7 analyzer at a heating rate of 10 °C/min. Refractive indices were determined on a J A Woollam Variable Angle Ellipometry System with a wavelength tunability from 300 to 1,700 nm. To fit the acquired Ψ and Δ curves with the data obtained from the 3-layer optical model consisting of crystalline silicon substrate, 2-nm SiO_2 layer and a uniform polymer film, the Levenberg–Marquardt regression algorithm was employed. The cauchy dispersion law was applied to describe the polymer layer from visible to IR region.

The X-ray photoelectron spectroscopy (XPS) experiments were conducted on a PHI 5600 spectrometer (Physical Electronics) and the core level spectra were measured using a monochromatic Al K_α X-ray source ($hv = 1386.6$ eV). The analyzer was operated at 23.5 eV pass energy and the analyzed area was 800 min diameter. The energy-dispersion X-ray (EDX) analyses were performed on a JOEL-6300 SEM system with quantitative elemental mapping and line scan capacities operating at an accelerating voltage of 15 kV. Morphologies of the ceramics were imaged on a JEOL-6300 scanning electron microscope (SEM) operating at an accelerating voltage of 15 kV. Structures of the ceramics were investigated by high-resolution transmission electron microscopy (HRTEM) JEOL 2010F TEM. The X-ray diffraction diagrams were recorded on a Philips PW 2830 powder diffractometer using monochromatized X-ray beam from a nickel-filtered Cu Kα radiation ($\lambda = 1.5406$ Å). Magnetization curves were recorded on a Lake Shore 7037/9509-P vibrating sample magnetometer at room temperature.

2.3 Monomer Preparation

*2.3.1 Preparation of (4-Methoxybenzyl)ferrocene (**5**)*

Into a 250 mL round-bottom flask were added 2.60 g (0.04 mol) of ferrocene (**3**), 2.76 g (0.02 mol) of 4-methoxybenzyl alcohol (**4**) and 100 mL of dry CH_2Cl_2. 6 mL of CF_3COOH was then added into the solution. After stirring at room temperature for 30 min, the mixture was poured into 150 mL of saturated aqueous solution of sodium bicarbonate. The aqueous phase was extracted with 50 mL CH_2Cl_2 five times and the organic layers were combined and concentrated by a rotary evaporator. The crude product was purified by a silica gel column using chloroform/hexane (1:1 v/v) as eluent. A red oil of **5** was obtained in 76.3 % yield. ^{1}H NMR (300 MHz, $CDCl_3$), δ (TMS, ppm): 7.10 (d, 2H), 6.82 (d, 2H), 4.16 (s, 5H), 4.09 (s, 4H), 3.77 (s, 3H), 3.62 (s, 2H). ^{13}C NMR (75 MHz, $CDCl_3$), δ (TMS, ppm): 157.8, 133.8, 129.3, 113.6, 88.5, 68.6, 68.5, 67.4, 55.2, 35.1.

*2.3.2 Preparation of (4-Hydroxybenzyl)ferrocene (**6**)*

Into a 250 mL round-bottom flask were added 4.59 g (0.015 mol) of **5** and 150 mL of dry CH_2Cl_2. 4.35 mL (0.045 mol) of BBr_3 was then added into the solution. After stirring at room temperature for 30 min, the mixture was poured into 150 mL of saturated aqueous solution of sodium bicarbonate. The aqueous phase was extracted with 50 mL CH_2Cl_2 five times and the organic layers were combined and concentrated by a rotary evaporator. The crude product was purified by a silica gel column using ethyl acetate/hexane (1:1 v/v) as eluent. Red solid of **6** was obtained in 72.3 % yield. ^{1}H NMR (300 MHz, $CDCl_3$), δ (TMS, ppm): 7.04 (d, 2H), 6.72 (d, 2H), 4.82 (s, 1H), 4.10 (s, 5H), 4.02 (s, 4H), 3.60 (s, 2H). ^{13}C NMR (75 MHz, $CDCl_3$), δ (TMS, ppm): 150.9, 147.5, 140.4, 129.4, 121.2, 87.7, 81.4, 74.3, 68.5, 68.3, 67.3, 34.7.

*2.3.3 Preparation of 4-(Ferrocenylmethyl)phenyl Propiolate (**2**)*

Into a 250 mL round-bottom flask were dissolved 10 mmol of **6**, 3.16 g (15.4 mmol) of DCC, 0.25 g (2.1 mmol) of

DMAP and 0.39 g (1.79 mmol) of TsOH in 100 mL of dry CH_2Cl_2. The solution was cooled to 0 °C with an ice–water bath, into which 0.7 g (10 mmol) of propiolic acid dissolved in 10 mL of dry CH_2Cl_2 was added under stirring via a dropping funnel. The reaction mixture was stirred overnight. After filtration, the solution was concentrated by a rotary evaporator. The crude product was purified by a silica gel column using chloroform/hexane (1:4 v/v) as eluent. Red solid of **2** was obtained in 75.8 % yield. ^{1}H NMR (300 MHz, DMSO-d_6), δ (TMS, ppm): 7.36 (d, 2H), 7.22 (d, 2H), 4.95 (s, 1H), 4.25 (s, 7H), 4.17 (s, 2H), 3.76 (s, 2H). ^{13}C NMR (75 MHz, DMSO-d_6), δ (TMS, ppm): 150.9, 147.5, 140.4, 129.4, 121.2, 87.7, 81.4, 74.3, 68.5, 68.3, 67.3, 34.7. Anal. Calcd for $C_{20}H_{17}O_2Fe$: C, 69.79, H, 4.69. Found: C, 69.34, H, 4.80.

2.4 Polymerization

All the polymerization reactions were carried out under nitrogen using a standard Schlenk technique. A typical procedure for the polymerization is given below: In a 15 mL Schlenk tube with a three-way stopcock on the side arm was placed 88.7 mg of **1** (0.267 mmol) and 0.18 g of **2** (0.534 mmol) under nitrogen in a glovebox. Distilled DMF (1.5 mL) was then added to dissolve the monomer using a hypodermic syringe. After stirring under reflux for 24 h, the mixture was added dropwise to ~300 mL of methanol through a cotton filter under stirring. The precipitates were allowed to stand overnight and then collected by filtration. The isolated polymer *hb*-P**1**/**2**c was washed with methanol and dried under vacuum at room temperature to a constant weight. *hb*-P**1**/**2**a and *hb*-P**1**/**2**b were prepared by the same procedures using molar ratios of [**2**]/[**1**] of 1.0 and 1.5, respectively. Their characterization data are shown below.

hb-P**1**/**2**a: Brown powder; yield 46.0 %. M_w 39,400; M_w/M_n 6.1 (GPC, polystyrene calibration). IR (thin film), ν (cm^{-1}): 3086, 3038, 2966, 2932, 2870, 2378, 1742, 1646, 1602, 1506, 1466, 1408, 1394, 1334, 1294, 1218, 1200, 1170, 1104, 1080, 1016. ^{1}H NMR (300 MHz, DMSO-d_6), δ (TMS, ppm): 9.31, 9.07, 7.37, 7.35, 7.11, 6.76, 4.26, 4.20, 3.77, 3.46, 1.77, 1.71. ^{13}C NMR (75 MHz, DMSO-d_6), δ (TMS, ppm): 171.6, 171.3, 171.0, 170.8, 170.7, 170.5, 170.2, 169.9, 163.0, 155.1, 148.1, 140.2, 136.2, 130.8, 129.3, 127.7, 121.3, 114.7, 68.5, 67.3, 34.7, 30.4.

hb-P**1**/**2**b: Brown powder; yield 41.3 %. M_w 25,300; M_w/M_n 4.9 (GPC, polystyrene calibration). IR (thin film), ν (cm^{-1}): 3089, 3037, 2967, 2929, 2869, 2851, 1743, 1645, 1601, 1505, 1465, 1435, 1409, 1385, 1363, 1333, 1295, 1219, 1201, 1169, 1105, 1081, 1017. ^{1}H NMR (300 MHz, DMSO-d_6), δ (TMS, ppm): 9.31, 9.07, 7.35, 7.11, 6.76, 4.29, 3.72, 3.49, 3.45, 1.77, 1.71. ^{13}C NMR (75 MHz, DMSO-d_6), δ (TMS, ppm): 171.6, 171.3, 171.1, 170.8, 170.5, 170.4, 169.9, 158.0, 151.1, 140.7, 136.0, 133.1, 130.2, 128.4, 123.5, 121.3, 118.7, 68.5, 67.8, 67.3, 32.9, 30.4.

hb-P**1**/**2**c: Brown powder; yield 34.3 %. M_w 16,400; M_w/M_n 3.8 (GPC, polystyrene calibration). IR (thin film), ν (cm^{-1}): 3086, 3038, 2966, 2930, 2870, 2854, 1894, 1742, 1644, 1622, 1602, 1504, 1464, 1438, 1410, 1486, 1364, 1336, 1292, 1220, 1200, 1168, 1104, 1080, 1040, 1016, 1000. ^{1}H NMR (300 MHz, DMSO-d_6), δ (TMS, ppm): 9.31, 9.07, 7.35, 7.12, 6.75, 4.74, 4.23, 4.21, 4.15, 3.78, 3.44, 1.76, 1.71. ^{13}C NMR (75 MHz, DMSO-d_6), δ (TMS, ppm): 171.2, 170.9, 170.7, 170.6, 170.3, 130.0, 169.7, 162.9, 155.1, 148.0, 139.9, 134.9, 130.8, 129.2, 127.6, 121.2, 114.7, 87.7, 67.3, 34.6, 30.4.

2.5 Photopatterning

Photo-cross-linking reactions of the polymer films were conducted in air at room temperature using the 365 nm light obtained from a Spectroline ENF-280C/F UV lamp at a distance of 1 cm as light source. The incident light intensity was ~18.5 mW/cm^2. The film was prepared by spin-coating the polymer solution (10 % w/w in 1,2-dichloroethane) at 2,000 rpm for 1 min on a silicon wafer. The polymer film was dried in a vacuum oven at room temperature overnight. The photoresist patterns were generated using copper photomasks and taken on an optical microscopy (Nikon 80i equipped with Nikon Digital Sight DS-5Mc-L2 Cooled CCD camera) using normal and UV light source.

3 Results and Discussion

3.1 Monomer Preparation

To explore the utilization of propiolate cyclotrimerization to construct processable metal-containing macromolecules, we adopted an $A_2 + B$ approach and used bipropiolate **1** and monopropiolate **2** as building blocks for the synthesis of organometallic *hb*-PTACPs. Whereas **1** was prepared according to the published procedures, **2** was synthesized by the synthetic route shown in Scheme 2. The monomer was characterized spectroscopically, from which satisfactory analysis data corresponding its molecular structure were obtained (see "Experimental" section for details). Single crystals of **2** were grown from its solution and analyzed by X-ray crystallography. Its ORTEP drawing is shown in Fig. 1 and the crystal data are summarized in Tables S1–S6 (Electronic supporting information).

3.2 Polymer Synthesis

In our previous studies, we found that aryl propiolates can undergo regioselective cyclotrimerization in reflux DMF

Scheme 2 Synthesis of ferrocene-containing monopropiolate **2**

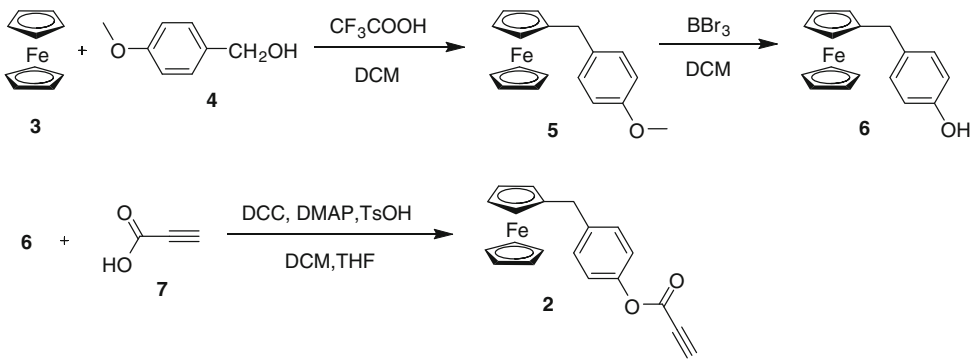

Fig. 1 ORTEP drawing of propiolate monomer **2** (CCDC 888125)

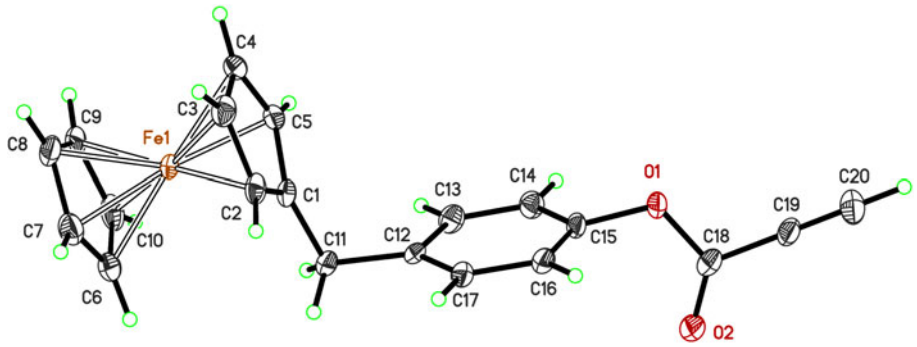

[22]. Thus, we employed the same condition for the polymerization of **1** and **2**. Different amounts of **2** are used for the polycyclotrimerization in order to fine tune the ferrocene content in the resulting polymers. All the polymerizations undergo smoothly, yielding polymers with high molecular weights in moderate yields (Table 1). The reddish-brown color of the polymers indicates that the ferrocene unit has indeed been introduced into the polymer structure. It is noteworthy that with an increase in the monopropiolate concentration or the molar ratio of [**2**]/[**1**], the yield and molecular weight of the resulting hyperbranched polymer are decreased accordingly. It is understandable because **2** functions as an end-capping reagent, which hampers the growth of the polymer chain when its concentration is raised. The M_w values of the polymers shown in Table 1 are probably considerably underestimated because of their hyperbranched nature coupled with their rigid structure [38, 39]. Our previous investigation reveals that the underestimation can be as large as 7–50-folds [40, 41]. The absolute molecular weights of the organometallic *hb*-PTACPs may thus be much larger than the relative values estimated from the GPC analysis.

Table 1 Copolymerization of bipropiolate **1** with monopropiolate **2**

Polymer	[**2**]/[**1**]	Yield (%)	M_w[a]	M_w/M_n[a]
hb-P**1**/**2**a	1	46.0	39,400	6.0
hb-P**1**/**2**b	1.5	41.3	25,300	4.9
hb-P**1**/**2**c	2	34.0	16,400	3.8

Carried out in reflux DMF for 24 h under nitrogen; [**1**] = 0.178 M

[a] Determined by GPC in THF on the basis of a linear polystyrene calibration

3.3 Structural Characterization

The polymers were characterized by spectroscopic methods with satisfactory results. An example of the IR spectra of *hb*-P**1**/**2**c and its monomers **1** and **2** are given in Fig. 2. The ≡C–H and C≡C stretching vibrations of **1** and **2** occur at 3,269 and 2,124 cm^{-1}, respectively, which disappear completely in the spectrum of its polymer. This indicates that the acetylene triple bonds of **1** and **2** have been consumed by the polymerization. Characteristic absorption bands of monosubstituted Fc are observed at 1,105 and 1,000 cm^{-1} in *hb*-P**1**/**2**c, confirming that the polycyclotrimerization reaction proceeds as expected and is not harmful to the Fc group.

Figure 3 shows the ^1H NMR spectra of *hb*-P**1**/**2**c, **1** and **2** in DMSO-d_6. The spectrum of *hb*-P**1**/**2**c shows no acetylene proton resonances of **1** and **2** at $\delta \sim 4.95$. The new resonance peaks at δ 9.29 and 9.06 represents the proton resonances of the benzene rings of the terminal and dendritic units of *hb*-P**1**/**2**c newly formed by the cyclotrimerization polymerization. No absorption peaks associated with the linear unit are observed. Thus, it is difficult for us to calculate the degree of branching of the polymer. The

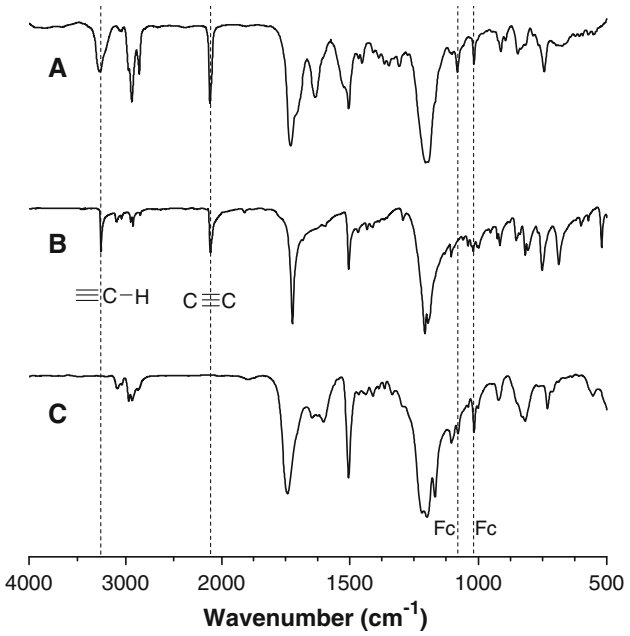

Fig. 2 IR spectra of (*A*) **1**, (*B*) **2** and (*C*) their polymer *hb*-P**1/2**c

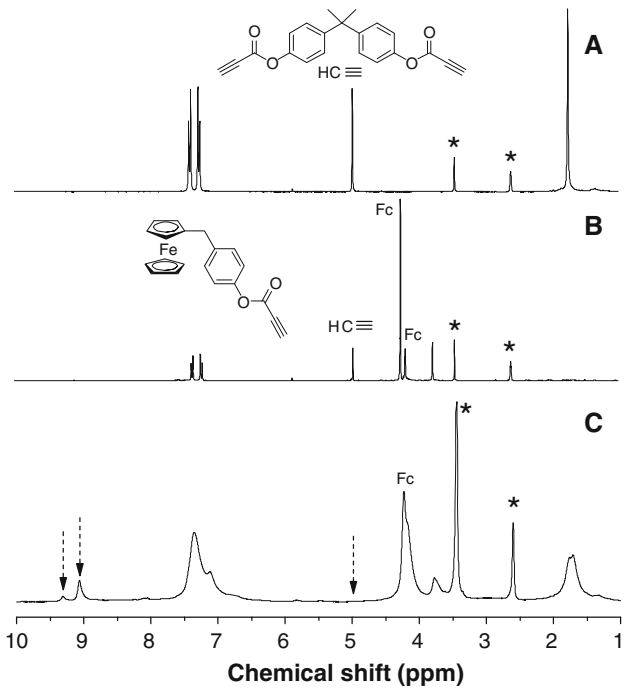

Fig. 3 ^{1}H NMR spectra of (*A*) **1**, (*B*) **2** and (*C*) *hb*-P**1/2**c in DMSO-d_6. The solvent and water peaks were marked with *asterisks*

peak at δ 4.23 represents the protons on the cyclopentadienyl ring of the ferrocene moiety, which further substantiates that **2** has been successfully incorporated into the polymeric structure. From its integral, the iron contents of *hb*-P**1/2**a, *hb*-P**1/2**b and *hb*-P**1/2**c are determined and equal to 5.82, 6.99 and 7.86 % respectively.

3.4 Solubility and Stability

All the hyperbranched polymers are completely soluble in common organic solvents, such as toluene, dichloromethane, chloroform, THF and dioxane, and can be readily fabricated into tough solid films by spin-coating and static-casting processes. They also enjoy high thermal stability, exhibiting 5 % loss (T_d) of their weight at around 300 °C under nitrogen (Fig. 4). Among the polymers, *hb*-P**1/2**c shows the highest weight residue (>30 %) when it is heated to 900 °C. This is probably due to its higher content of Fc unit, which well wraps the polymer chain and thus protects it from the attack by the degradative species. The high ceramic yields of the polymers suggest that they are promising candidates as precursors to magnetoceramic materials.

3.5 UV Absorption and Light Refraction

The UV spectra of *hb*-P**1/2** in THF solutions are shown in Fig. 5. All the polymers exhibit a board absorption band at 400–550 nm, which is assignable to the d–d transition within the ligand field formalism of the conjugated ferrocene.

Our previous studies show that *hb*-PTACPs show high RI or n values due to the presence of large amount of polarizable aromatic rings and ester groups [22]. With the incorporation of Fc moieties into the polymer structure, the organometallic *hb*-PTACPs may show even high RI values. Indeed, as shown in Fig. 6, *hb*-P**1/2**c displays high refractivity (n = 1.7038–1.6448) in a wide spectroscopic

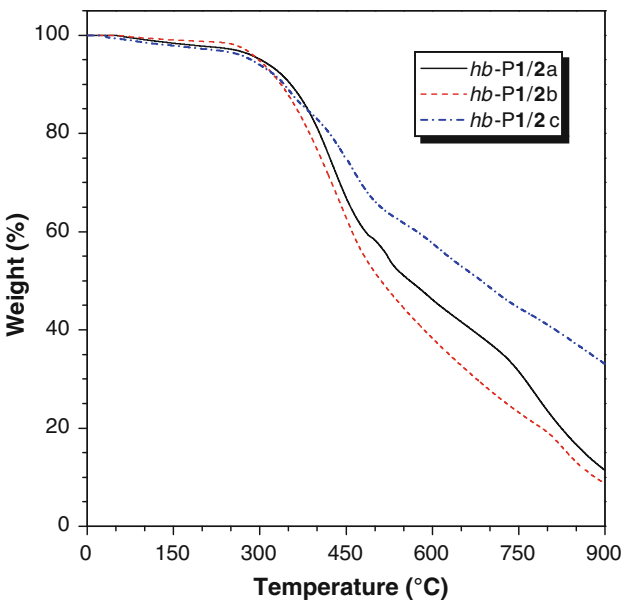

Fig. 4 TGA thermograms of hyperbranched polymers *hb*-P**1/2** recorded under nitrogen at a heating rate of 10 °C/min

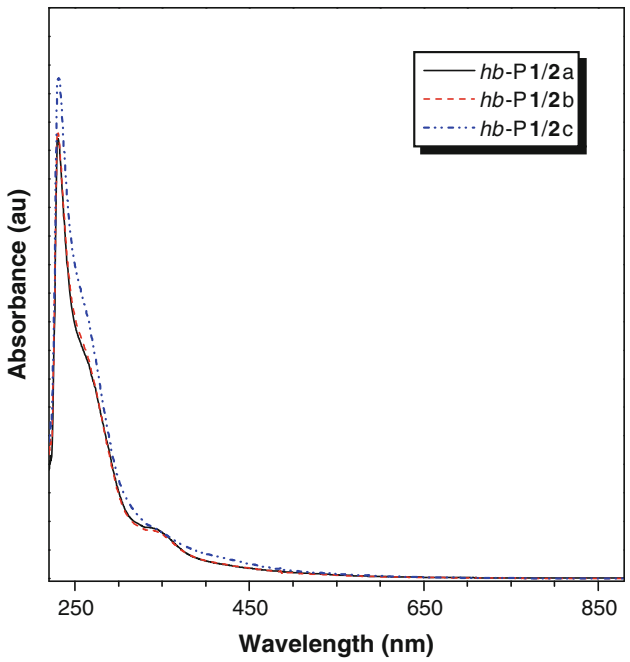

Fig. 5 Absorption spectra of *hb*-P**1/2** in THF solutions. Concentration: 0.03 mg/mL

region (400–1,700 nm). The RI values ($n = 1.6900$–1.6295) of *hb*-P**1/2**a and *hb*-P**1/2**b are slightly lower than those of *hb*-P**1/2**c at the same spectral region because of their lower Fc content but are still much higher than those of commercial optical glasses. Clearly, the ferrocene-functionalized *hb*-PTACPs are a class of highly refractive polymers. No or little birefringence is detected, which is indicative of the amorphous nature of the polymer films. It is noteworthy that the RI difference between the polymers at the telecommunication important wavelength of 1,550 nm can be as large as 0.0153, suggesting that the photonic properties of the organometallic *hb*-PTACPs can be tuned readily by simply changing the monomer feed ratio in the polymerization.

For materials to be useful for practical applications, its optical aberration should be small enough. The Abbé number (v_D) of a material is a measure of the variation or dispersion in its RI value with wavelength and is defined as: $v_D = (n_D - 1)/(n_F - n_C)$, where n_D, n_F and n_C are the RI values at wavelengths of Fraunhofer D, F and C spectral lines of 589.2, 486.1 and 656.3 nm, respectively. A modified Abbé number (v'_D) has been proposed to evaluate the application potential of an optical material, using its RI values at the non-absorbing wavelengths of 1064, 1319 and 1550 nm [42, 43]. The first two wavelengths are chosen in view of the practical interest of commercial laser wavelengths (Nd:YAG), while the last one is the wavelength for telecommunication. The modified Abbé number is defined as: $v'_D = (n_{1319} - 1)/(n_{1064} - n_{1599})$, where n_{1319}, n_{1064} and n_{1550} are the RI values at 1319, 1064, and 1550 nm, respectively. The chromatic dispersion ($D^{(\prime)}$) is the constringence of the Abbé number ($v_D^{(\prime)}$) and is defined as: $D^{(\prime)} = 1/v_D^{(\prime)}$. All the polymers exhibit similar low D and D' values of 0.029 and $\sim$0.007, respectively (Fig. 6), suggesting that they possess good chromatic dispersion. Coupled with their high RI values, they are thus potential candidates for advanced optical devices.

3.6 Ceramization

The high ceramics yields of *hb*-P**1/2** encourage us to utilize them as precursors to magnetic ceramics. Pyrolysis of the organometallic polymers in tube furnaces at 900 °C for 1 h under a steam of nitrogen gives ceramics products C**1**–C**3** in 27.4, 48.8 and 52.0 % yields, respectively (Scheme 3).

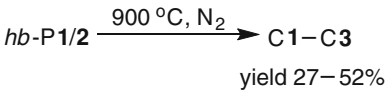

Scheme 3 Ceramization to magnetic ceramics

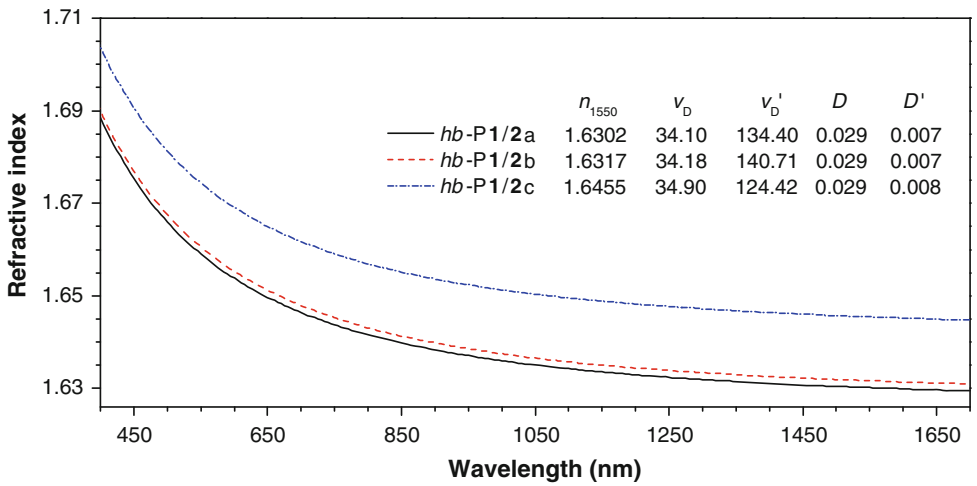

Fig. 6 Wavelength dependence of refractive index of thin films of *hb*-P**1/2**

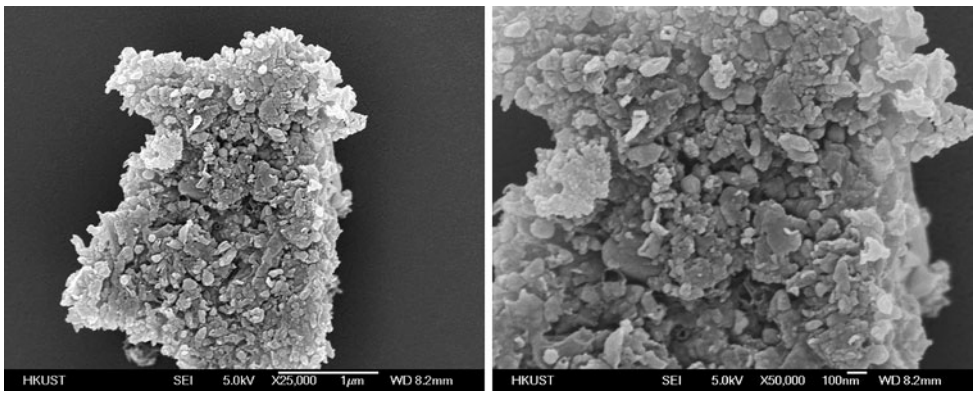

Fig. 7 SEM images of ceramics C**1** prepared by pyrolytic ceramization of *hb*-P**1**/**2**a at 900 °C under nitrogen

Table 2 Compositions of the ceramics estimated by XPS and EDX analyses

Ceramics	XPS (%)			EDX (%)		
	C	Fe	O	C	Fe	O
C1	94.38	0.86	4.51	80.65	10.90	8.45
C2	89.82	1.76	7.50	75.85	21.96	2.19
C3	87.01	2.53	9.26	51.42	32.82	15.76

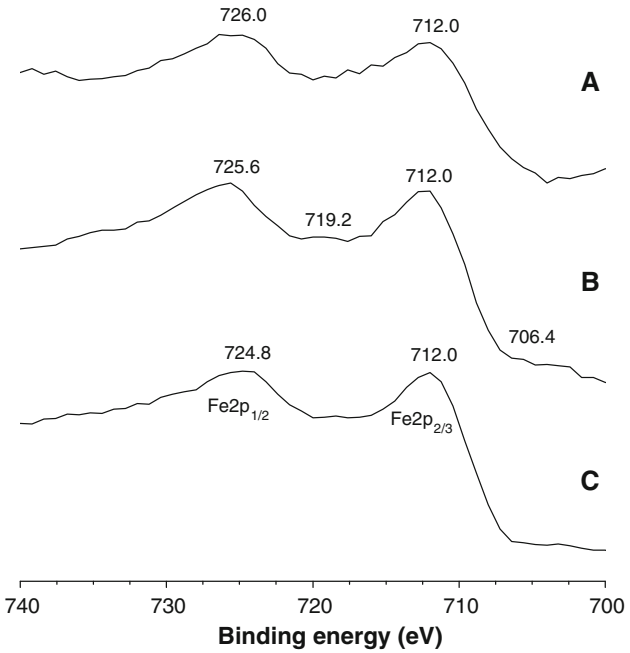

Fig. 8 Fe2p photoelectron spectra of (*A*) C**1**, (*B*) C**2** and (*C*) C**3**

All the ceramics are magnetizable and can be readily attracted to a bar magnet at room temperature.

3.7 Structure and Composition

To get a first impression of the prepared metalloceramics, we used SEM to investigate their surface morphology. Figure 7 shows the SEM image of C**1** as an example. The

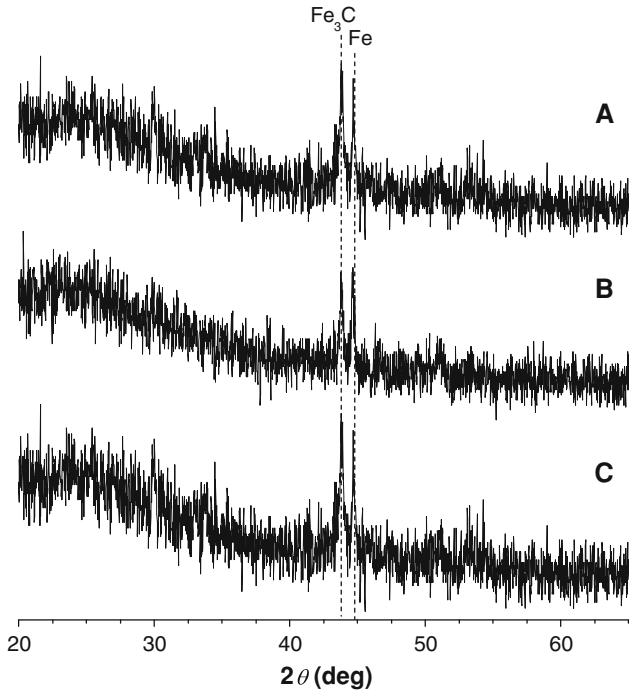

Fig. 9 XRD diffractograms of (*A*) C**1**, (*B*) C**2** and (*C*) C**3**

ceramics produced at 900 °C under an atmosphere of nitrogen are compact but rough materials, decorated with only small particles and clusters. Such morphology suggests a good heat-resistance of the organometallic *hb*-PTACPs, stripping off only small amounts of volatile fragments during the harsh conditions of the ceramization process [44].

We then carried out XPS and EDX analyses to estimate the chemical compositions of the ceramics (Table 2). XPS measurements give iron contents of 0.86, 1.76 and 2.53 % on the surfaces of C**1**, C**2** and C**3**, respectively. In the bulk, the contents are respectively changed to 10.90, 21.96 and 32.82 %. The composition gradient of the transition metal from bulk to the surface implies that the ceramization process starts from the formation of the iron nanocluster cores and end by the wrapping with carbon coronas.

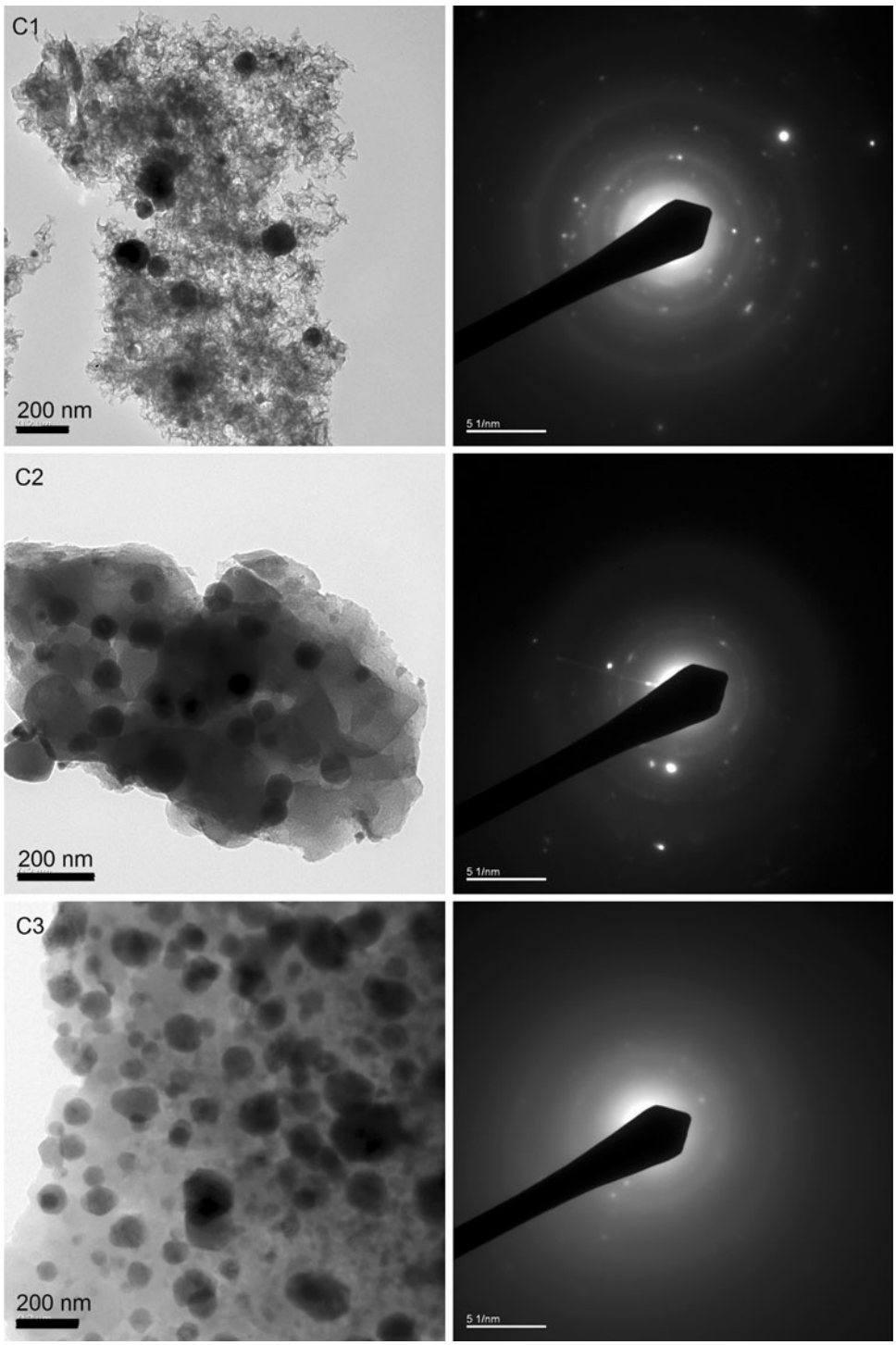

Fig. 10 (*Left*) HRTEM images and (*right*) ED patterns of ceramics C**1**, C**2** and C**3**

XPS analysis provides further information on the chemical structures of the surfaces of the ceramic products [45]. From the magnified Fe2p photoelectron spectra of C**1**–C**3** shown in Fig. 8, two major peaks associated with the $Fe2p_{1/2}$ and $Fe2p_{2/3}$ core level binding energies of Fe_2O_3 are observed at ~725 and 712 eV, respectively. A weak absorption peak also appears at 719 eV in the spectrum of C**2**. Allen et al. [46] and Fradley [47] reported a binding energy of Fe at 720.3 eV. Thus, the emergence of such shoulder demonstrates the presence of metallic iron on the surface of C**2**.

In order to gain more insights into the chemical compositions of the bulk of C**1**–C**3**, we further investigated our ceramics by XRD analysis. Figure 9 shows the XRD patterns of C**1**–C**3**. All the ceramics exhibit Bragg reflection peaks at 2θ angles of 43.8°, and 44.7°, suggesting that they

all contains crystalline species. The reflection peaks can be identified according to the databases of JCPDS-International Centre for Diffraction Data (ICDD) as reflections for the iron metal of Fe_3C and Fe (ICDD data file 23-1113 and 06-0696, respectively).

The structures of the nanocrystallites of C**1**–C**3** are studied by HRTEM analysis. As shown in Fig. 10, the iron nanoparticles (dark grains) are of irregular round shape and well embedded in the abundant carbon matrix (light areas). The sizes of the nanoparticles range from 200 to ~50 nm. Fe is known to catalyze the crystallization and the formation of nanotubes. From the TEM pictures, it is clear that the Fe nanoparticles are covered by the graphite sheets, which may act as protective coating of the nanoparticles toward oxidation. The ED patterns of the ceramics further suggests their crystalline nature.

3.8 Magnetism

Because the ceramic materials contain nanoscopic iron species, they are expected to be magnetically susceptible. As shown in Fig. 11, the magnetization of C**1**, C**2** and C**3** swiftly increases and ultimately saturates at ~14, 11 and 7 emu/g, respectively. The higher saturation magnetization of C**1** may be associated with its larger iron nanoparticles with higher crystallinity, as suggested by its HRTEM image shown in Fig. 10.

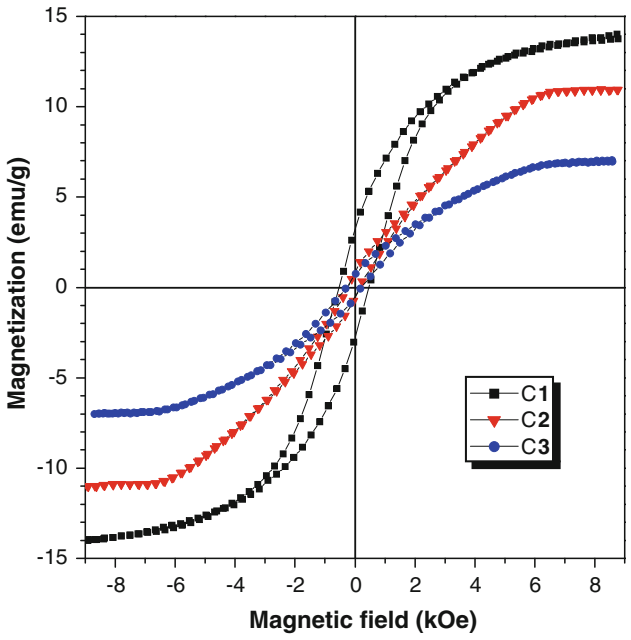

Fig. 11 Plots of magnetization versus applied magnetic field at 300 K for ceramics C**1**, C**2** and C**3** prepared by pyrolysis at 900 °C under nitrogen

3.9 Photopatterning

The *hb*-PTACPs synthesized in our previous work are sensitive photoresist materials due to the presence of vast number of aromatic esters units in their structures [22]. Indeed, UV irradiation of a thin film of *hb*-P**1**/**2**a spin-coated on a silicon wafer in air through a copper mask results in cross-linking of the exposed region, while the covered parts render soluble. A negative photoresist pattern is thus generated after development in 1,2-dichloroethane (Fig. 12a).

Magnetoceramic pattern can be generated by pyrolysis the patterned polymer film at 900 °C under nitrogen atmosphere for 1 h. As shown in Fig. 12b, no significant change in the resulting ceramic pattern is observed with respect to the polymer precursor. The rough surfaces of the lines indicate a transformation of the surface topology of the patterned area from a uniform thin film to a collection of small ceramic particles. The composition of these particles is probably comparable with that of C**1** in the bulk,

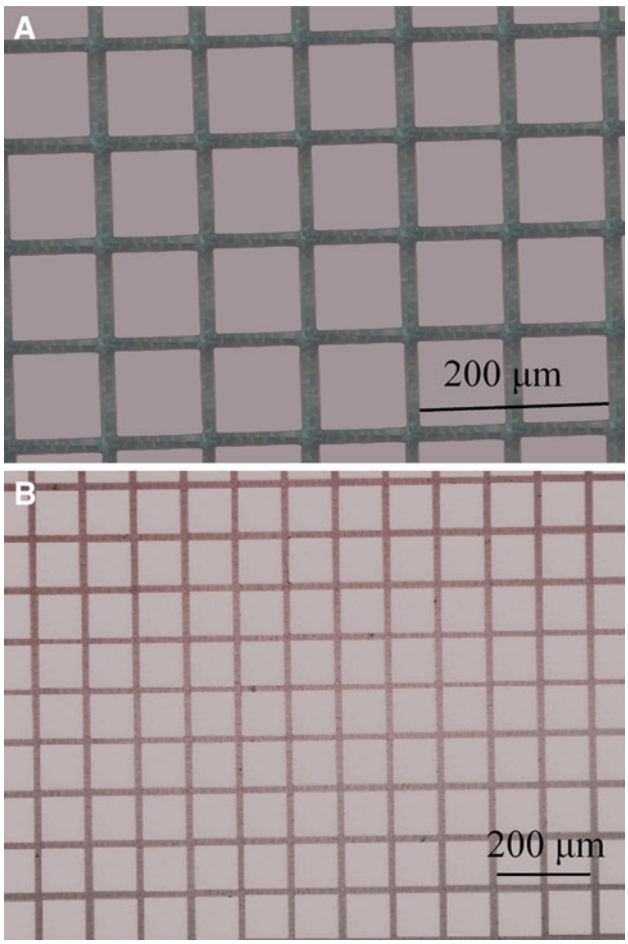

Fig. 12 **a** Negative photoresist pattern generated by photolithography of *hb*-P**1**/**2**a. **b** Magnetoceramic pattern generated by pyrolysis of the negative photoresist pattern of *hb*-P**1**/**2**a at 900 °C under nitrogen for 1 h

which contains iron-rich nanocrystallites well embedded in the abundant graphite matrix. It shows a good example of combining conventional lithographic techniques with easily processable organometallic polymer resists [48].

4 Conclusion

In this work, organometallic *hb*-PTACPs with high molecular weights are synthesized in moderate yields by polycyclotrimerization of **1** and **2** in reflux DMF. The resulting polymers are completely soluble, film-forming and thermally stable. Their metal content can be tuned readily by varying the monomer feed ratio in the polymerization. Their thin films show high refractive indices of 1.7038–1.6295 in the spectral region of 400–1,700 nm. The organometallic polymers are excellent precursors to iron-containing ceramics. Ceramization of *hb*-P**1/2** at 900 °C under nitrogen gives iron nanocrystallites with high magnetic susceptibility in good yield. The polymers are readily crosslinked under UV irradiation to generate photoresist patterns. Pyrolysis of the patterned polymer film produces magnetoceramic pattern with good shape retention.

Acknowledgments The work reported in this paper was partially supported by the National Science Foundation of China (20974028), the RPC and SRFI Grants of HKUST (RPC10SC13, RPC11SC09 and SRFI11SC03PG), the Research Grants Council of Hong Kong (604711, 603509, HKUST2/CRF/10 and N_HKUST620/11), the Innovation and Technology Commission (ITCPP/17-9) and the University Grants Committee of Hong Kong (AoE/P-03/08).

References

1. J. Liu, M. Ueda, J. Mater. Chem. **19**, 8907 (2009)
2. N. You, C. Chueh, C. Liu, M. Ueda, W.C. Chen, Macromolecules **42**, 4456 (2009)
3. S. Kusaka, R. Sakamoto, Y. Kitagawa, M. Okumura, H. Nishihara, Chem. Asia J. **7**, 907 (2012)
4. M. Hayashi, F. Toshimitsu, R. Sakamoto, H. Nishihara, J. Am. Chem. Soc. **133**, 14518 (2011)
5. K. Uchida, Y. Yamanoi, T. Yonezawa, H. Nishihara, J. Am. Chem. Soc. **133**, 9239 (2011)
6. I. Nakamula, Y. Yamanoi, T. Imaoka, K. Yamamoto, H. Nishihara, Angew. Chem. Int. Ed. **50**, 5830 (2011)
7. S. Kume, H. Nishihara, Chem. Commun. **47**, 415 (2011)
8. H. Kondo, Y. Yamanoi, H. Nishihara, Chem. Commun. **47**, 6671 (2011)
9. Y. Hasegawa, K. Takahashi, S. Kume, H. Nishihara, Chem. Commun. **47**, 6846 (2011)
10. S. Muratsugu, K. Sodeyama, F. Kitamura, S. Tsukada, M. Tada, S. Tsuneyuki, H. Nishihara, Chem. Sci. **2**, 1960 (2011)
11. K. Namiki, M. Murata, S. Kume, H. Nishihara, New J. Chem. **35**, 2146 (2011)
12. K.P. Rao, T. Kusamoto, F. Toshimitsu, K. Inayoshi, S. Kume, R. Sakamoto, H. Nishihara, J. Am. Chem. Soc. **132**, 12472 (2010)
13. Z.Q. Qin, M.C. Jennings, R.J. Puddephatt, Chem. Commun. **4**, 1354 (2002)
14. M.C. Brandys, R.J. Puddephatt, J. Am. Chem. Soc. **124**, 3946 (2002)
15. T.J. Burchell, R.J. Puddephatt, Inorg. Chem. **44**, 3718 (2005)
16. J.C. Seferis, in *Polymer Handbook*, 3rd edn., ed. by J. Brandrup, E.H. Immergut (Wiley, New York, 1989), pp. VI/451–VI/461
17. W.Z. Yuan, R. Hu, J.W.Y. Lam, N. Xie, C.K.W. Jim, B.Z. Tang, Chem. Eur. J. **18**, 2847 (2012)
18. C.K.W. Jim, A. Qin, F. Mahtab, J.W.Y. Lam, B.Z. Tang, Chem. Asia J. **6**, 2753 (2011)
19. P. Lu, J.W.Y. Lam, J. Liu, C.K.W. Jim, W. Yuan, C.Y.K. Chan, N. Xie, Q. Hu, K.K.L. Cheuk, B.Z. Tang, Macromolecules **44**, 5977 (2011)
20. J. Liu, J.W.Y. Lam, C.K.W. Jim, J. Ng, Y. Cheuk, J. Shi, H. Su, K.F. Yeung, Y. Hong, F. Mahtab, Y. Yu, K.S. Wong, B.Z. Tang, Macromolecules **44**, 68 (2011)
21. C.K.W. Jim, A. Qin, J.W.Y. Lam, F. Mahtab, Y. Yu, B.Z. Tang, Adv. Funct. Mater. **20**, 1319 (2010)
22. C.K.W. Jim, A. Qin, J.W.Y. Lam, M. Häuβler, J. Liu, M.M.F. Yuen, J.K. Kim, K.M. Ng, Macromolecules **42**, 4099 (2009)
23. A. Qin, L. Tang, J.W.Y. Lam, C.K.W. Jim, Y. Yu, H. Zhao, J. Sun, B.Z. Tang, Adv. Funct. Mater. **19**, 1891 (2009)
24. K.C. Krogman, T. Druffel, M.K. Sunkara, Nanotechnology **16**, 338 (2005)
25. C. Lue, Z. Cui, Z. Li, B. Yang, J. Shen, J. Mater. Chem. **13**, 526 (2003)
26. R.A. Minns, R.A. Gaudiana, J. Macromol. Sci. Pure Appl. Chem. **A29**, 19 (1992)
27. Y. Terui, S. Ando, J. Photopolym. Sci. Technol. **18**, 337 (2005)
28. S. Wu, Y. Chen, F. Zeng, S. Gong, Z. Tong, Macromolecules **39**, 6796 (2006)
29. S. Nlate, J. Ruiz, D. Astruc, J.C. Blais, Chem. Commun. 417 (2000)
30. M. Even, B. Heinrich, D. Guillon, D.M. Guldi, M. Prato, R. Deschenaux, Chem. Eur. J. **7**, 2595 (2001)
31. M.M. Abd-Elzaher, W.H. Hegazy, A.E. Gaafar, Appl. Organomet. Chem. **19**, 911 (2005)
32. A.S. Adb-El-Aziz, C.E. Carraher, C.U. Pittman, J.E. Sheats, M. Zeldin (eds.), *Macromolecules Containing Metal and Metal-Like Elements, Transition Metal-Containing Polymers* (Wiley, Hoboken, 2004)
33. D.A. Foucher, B.Z. Tang, I. Manners, J. Am. Chem. Soc. **114**, 6246 (1992)
34. R. Petersen, D.A. Foucher, B.Z. Tang, A. Lough, N. Raju, J. Greedan, I. Manners, Chem. Mater. **7**, 2045 (1995)
35. C. Kloninger, M. Rehahn, Macromolecules **37**, 1720 (2004)
36. H.B. Eitouni, N.P. Balsara, J. Am. Chem. Soc. **126**, 7446 (2004)
37. K. Temple, K. Kulbaba, K.N. Power-Billard, I. Manners, K.A. Leach, T. Xu, T.P. Russell, C.J. Hawker, Adv. Mater. **15**, 297 (2003)
38. Z. Muchtar, M. Schappacher, A. Deffieux, Macromolecules **34**, 7595 (2001)
39. K.E. Uhrich, C.J. Hawker, J.M.J. Frechet, S.R. Turner, Macromolecules **25**, 4583 (1992)
40. R.H. Zheng, H.C. Dong, H. Peng, J.W.Y. Lam, B.Z. Tang, Macromolecules **37**, 5196 (2004)
41. H. Peng, L. Cheng, J. Luo, K. Xu, Q. Sun, Y. Dong, F. Salhi, P.P.S. Lee, J. Chen, B.Z. Tang, Macromolecules **35**, 5349 (2002)
42. C.J. Yang, S.A. Jenekhe, Chem. Mater. **7**, 1276 (1995)
43. C.J. Yang, S.A. Jenekhe, Chem. Mater. **6**, 196 (1994)
44. R.J.P. Corriu, Angew. Chem. Int. Ed. **39**, 1376 (2000)
45. P. Mills, J.L. Sullivan, J. Phys. D Appl. Phys. **14**, 723 (1983)
46. G. Allen, M. Curtis, A.J. Hopper, P.M. Tucker, J. Chem. Soc. Dalton Trans. **14**, 1525 (1974)
47. C.S. Fradley, in *Electron Spectroscopy*, ed. by D.A. Shurley (North-Holland, Amsterdam, 1972), p. 781
48. A.Y. Cheng, S.B. Clendenning, G. Yang, I. Manners, Chem. Commun. 780 (2004)